Hindawi
Shock and Vibration
Volume 2023, Article ID 8818380, 11 pages
https://doi.org/10.1155/2023/8818380

Research Article

Vibration Signal Analysis of Roadheader Based on Referential Manifold Learning

Hai Jiang[1], **Xiaodong Ji**[2], **Yang Yang**[3], **Yuanyuan Qu**[1] and **Miao Wu**[1]

[1]*China University of Mining and Technology, Beijing 100083, China*
[2]*Shijiazhuang Tiedao University, Shijiazhuang 050043, China*
[3]*Shijiazhuang Coal Mining Machinery Co., Ltd., Shijiazhuang 050000, China*

Correspondence should be addressed to Xiaodong Ji; jibaiyi@126.com

Received 30 April 2023; Revised 31 July 2023; Accepted 4 September 2023; Published 20 September 2023

Academic Editor: Xavier Chiementin

Roadheader is important large equipment in coal mining. The roadheader has a higher failure rate due to its harsh working environment and high working intensity. In this paper, we proposed a fault diagnosis method based on reference manifold (RM) learning by using the vibration signals of roadheader in the actual production process. First, health and fault vibration signals were extracted from a large number of field data. The abovementioned signals were analyzed by time domain and wavelet packet energy analysis and got the characteristic parameters of the signal which can form the characteristic parameter sets. RM method can reduce the dimension of the characteristic parameters, and the projection of different characteristic parameters was obtained. Finally, the health parameters and fault parameters of different characteristic parameters were segmented by linear discriminant analysis (LDA). It could get the different segment area range of characteristic parameters for health signals and fault signals. This method provides a set of fault analysis ideas and methods for equipment working under complex working conditions and improves the theoretical basis for fault type analysis.

1. Introduction

As a prerequisite of coal mining, the efficiency and quality of coal mine tunneling seriously affect the production progress and capacity of the mine [1]. Therefore, the reliability and continuous workability of roadheader have become the inevitable trend of roadheader research. In the past 20 years of mining of China, the development of roadheader has experienced the introduction of foreign technology, the self-development of small roadheader, the manufacture of high-power and high-load roadheader, and the successful development of today's multiauxiliary roadheader [2, 3]. The manufacture and use of the whole roadheader has reached a certain height, but due to the different physical characteristics of coal seams, the different characteristics of roof, the different operation habits of operators, and the diversification of geological conditions of rock roadway in different regions of China, there are still a variety of different problems in the use of roadheader: blockage and heating of hydraulic system; failure of electrical equipment; and damage of transmission parts and hydraulic pumps and motors. These problems seriously affect the working efficiency and progress of the roadheader. With the urgent requirements of the in-depth application and development of fully mechanized mining technology in the coal mines, efficient roadway driving is gradually regarded as one of the common and key technologies to realize efficient intensive production in coal mine. Therefore, the driving equipment with high automation, high reliability, and long life is an important prerequisite to ensure the safe and efficient forming of the roadway.

Vibration signal analysis is a common method of fault diagnosis [4]. At present, there had been some research on the vibration signal analysis of roadheader at home and abroad. Comakli studied the influence of physical and mechanical properties of tuff on the running state of roadheader [5]; Acaroglu and Erdogan compared and analyzed the vibration characteristics and stability of the

cutting head of the roadheader under different cutting modes [6]; Sun et al. solved the mode of the gearbox of the cutting part of the roadheader through ANSYS and finally obtained the vibration modal characteristics of the box of the reducer [7]; Wang build an excitation test system composed of vibration excitation equipment, vibration picking equipment, and data acquisition and analysis equipment and obtained the natural frequency distribution area of the whole roadheader and the vibration characteristics of the rocker arm and electric control box [8]. The abovementioned analysis of vibration signals of tunneling equipment is carried out based on theoretical analysis and simulation tests. Although it provided some theoretical support for the fault analysis of roadheader, it lacked actual downhole operation data as support. Based on those, Hu et al. analyzed the vibration signal of the roadheader collected by the vibration recorder and obtained the vibration intensity distribution of the roadheader, and the vibration of the cutting part was the strongest [9]; Yang and others used the fault data of roadheader turntable to propose a roadheader anomaly detection method based on VSAP-SO-BP under single-class learning, and the detection accuracy is 91.7% [10]. Qu et al. used a double complex wavelet (DTCWT) to analyze the measured vibration data of roadheader turntable, obtained the natural frequency of roadheader turntable under actual working conditions, and verifies the feasibility of applying modal identification theory to roadheader vibration signal processing under complex working conditions [11].

Wang proposed a new noise-assisted method, called EMD manifold (EMDM), for enhanced fault diagnosis of rotating machines [4]. Ding developed an improved fast TFM (FTFM) method to effectively and efficiently extract the transient characteristics of rotating machinery fault diagnosis [12]. Most of the research of manifold learning about mechanical fault diagnosis is on rotating machinery, such as bearings, gears, and so on. There are few studies of large machinery.

In the traditional vibration feature analysis process, the sensitive feature parameters were generally extracted based on the traditional time domain, frequency domain, wavelet analysis methods, and the characteristic parameters were compared to get the difference of different signals. Preliminary diagnosis of equipment faults can be completed through the abovementioned analysis [13–15]. Based on the previous research, combined with the traditional analysis method, this paper uses the characteristic parameters of the vibration signal as the data analysis feature set (to create the time domain and frequency domain characteristic parameter set of the vibration signal), then through manifold learning, the parameter set is reduced to extract more accurate sensitive parameters, and the data are divided into regions by linear recognition to achieve the purpose of identifying the fault state.

2. Fault Analysis Scheme Based on Feature Reference

The technical route of the vibration data analysis method is shown in Figure 1. First, the reference health data and analysis data are extracted from the vibration data collected on the cutting part of the roadheader as the initial data set of the analysis. Second, the characteristics of the data are obtained by time-frequency and wavelet analysis [15, 16], and the characteristic set of reference samples is constructed with reference to the eigenvalue set of health data and analysis data. Then, the LLE nonlinear popular learning is used to get the popular clustering space, and the low-dimensional feature space graph is used to describe and analyze the fault analysis results. Finally, linear discriminant analysis (LDA) is used to analyze the interclass divergence and intraclass divergence of low-dimensional feature space, and a thick linear discriminant clustering space is obtained, which can effectively segment fault signals from health data.

3. Vibration Signal Acquisition

3.1. On-the-Spot Situation. The experimental site was the Xingdong Coal Mine of Jizhong Energy. The coal of the mine is mainly gas and fat coal with high calorific value, and the coal seam is deep between 580 and 1200 m underground. The roadway excavated by the roadheader is the material transport roadway in the southern mining area of Xingdong Coal Mine 1100, and the roadway section is the trapezoid shown in Figure 2, which is the same as the coal seam section. The driving length is 200 m; there are no geological changes such as faults and gangue in the process of driving, and the trend of the roadway is shown in Figure 3.

The roadheader is an EBZ160 cantilever roadheader. The maximum cutting section of the roadheader is 5300×4850 mm. The cutting part of the roadheader is mainly composed of a gun head, a telescopic part, a cutting motor, a reducer, a telescopic hydraulic cylinder, and a shell [17], as shown in Figure 4. The transmission box is a two-stage planetary gear reducer, which drives the cutting head to rotate through the output shaft to realize the cutting function, and its transmission ratio is 31.03.

3.2. Vibration Measuring Point Arrangement. According to the working environment and load conditions of the roadheader, a total of 5 measuring points are arranged near the cutting part of the roadheader, each measuring point has 2 vibration sensors in different directions, a total of 10 sensors. The specific location of the sensor is shown in Figure 5 and Table 1. The sampling frequency of vibration data is 10 kHz and the sampling time was 32 days.

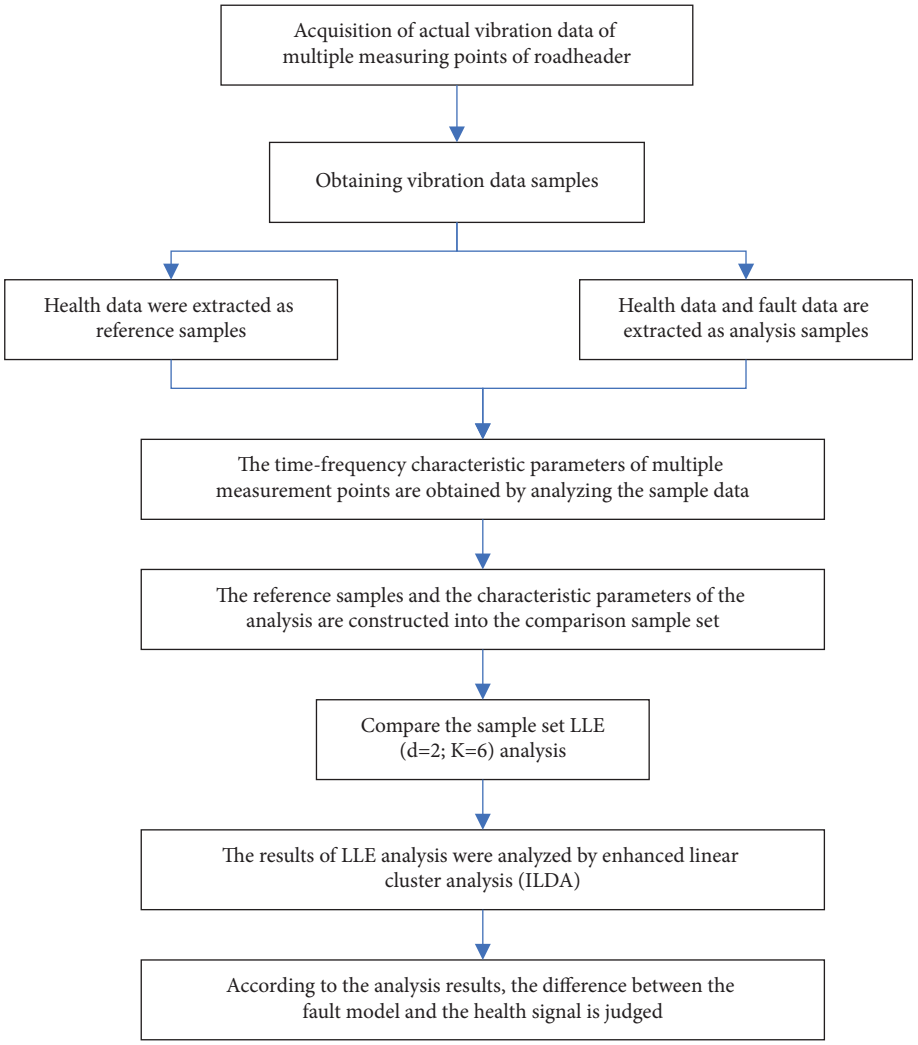

Figure 1: Analysis method flow.

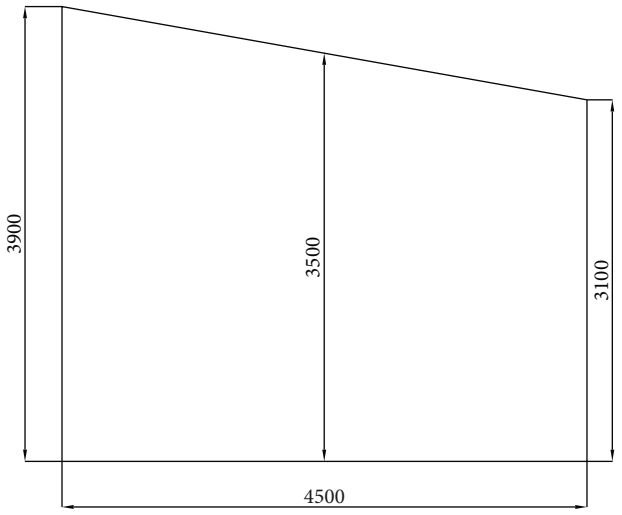

Figure 2: Schematic of section.

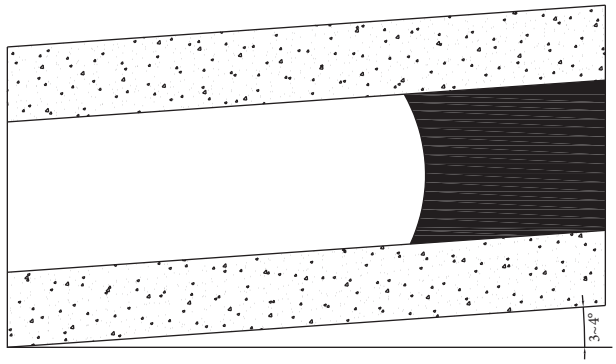

Figure 3: The roadway shape.

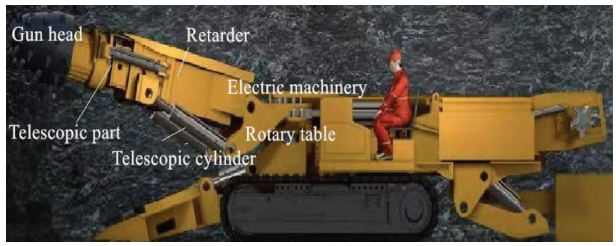

Figure 4: Roadheader.

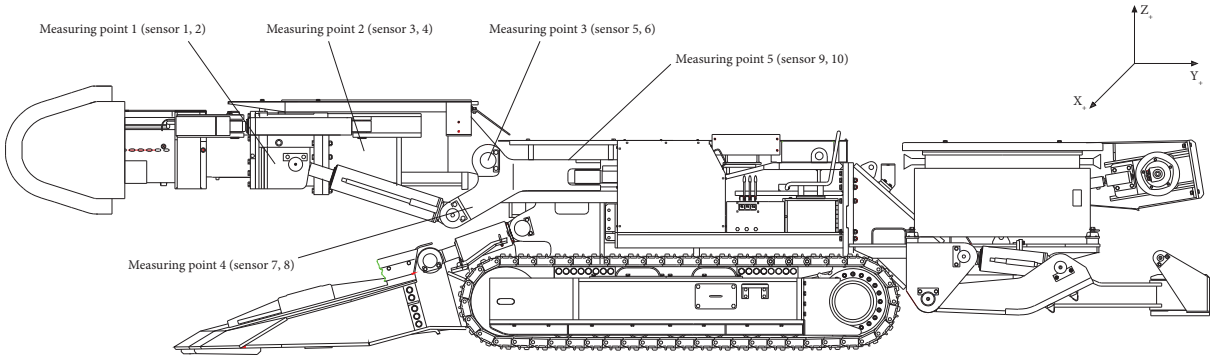

Figure 5: Arrangement drawings of roadheader's measuring point.

4. Construction of Feature Parameter Comparison Sample Set

According to the working records of the working site of the roadheader, it is known that a mechanical failure occurred in the cutting arm of the roadheader in the course of working for 32 consecutive days, and the gear of the reducer of the cutting arm of the roadheader was worn and broken due to overload. The marking A point in Figure 4 is the fault location.

In the traditional vibration data analysis, some sensitive characteristic signals are extracted from the vibration signals based on some data processing methods and statistical methods for comparison and experience summary. In this paper, the features extracted by traditional analysis (kurtosis, wavelet entropy, band energy, and time-frequency features) are used as the original features for reference manifold spatial clustering analysis [18–21]. The roadheader health signal and fault signal are effectively separated to achieve the purpose of fault diagnosis. 160 sets of vibration data are extracted from 8 healthy running periods and 8 groups of fault running periods of 10 sensors at 5 measuring points.

The 160 groups of data were analyzed in the time domain, frequency domain, and wavelet packet, respectively. The time-frequency characteristic parameters of each group of data are extracted: peak-to-peak value, effective value, absolute mean value, mean square deviation, kurtosis value, margin factor, peak factor, waveform factor, and 8 groups of energy ratios of 4-level wavelet analysis, as shown in Table 2:

According to the analysis of the parameters of the vibration sensor signal, the characteristic parameter sets of different periods are constructed, respectively. Taking the peak and peak values as an example, the peak and peak values of 10 sensors in the same period are extracted to construct an array: $x_i = (\mathrm{pk1}, \mathrm{pk2}, \ldots \mathrm{pk10})^T$. Among them, $i = (1, 2, \ldots, 16)$ represents 16 different periods. Then, the

Table 1: Corresponding relation of vibration sensor.

Measuring point	Measuring point position	Sensor direction	Sensor	Coordinate
1	Lifting cylinder support point	Perpendicular to the cutting arm (X)	1	
		Horizontal to the cutting arm (Y)	2	
2	Cutting gearbox	Perpendicular to the cutting arm (X)	3	
		Horizontal to the cutting arm (Y)	4	Establish the coordinate system according to the roadheader::
3	Hinge point between cutting part and turntable	Perpendicular to the cutting arm (X)	5	X: perpendicular to the side of the cutting part
		Horizontal to the cutting arm (Y)	6	Y: horizontal to the heading direction of the roadheader
4	Fixed points of lifting cylinder and turntable	Perpendicular to the cutting arm (X)	7	Z: perpendicular to the upper plane of the roadheader
		Horizontal to the cutting arm (Y)	8	
5	Turntable center	Horizontal and roadheader direction (Y)	9	
		Vertical roadheader upper plane (Z)	10	

Table 2: Characteristic parameters.

Time domain features	Mark symbol	Wavelet analysis feature	Mark symbol
Peak and peak value	pk	Energy ratio1	E1
Effective value	st	Energy ratio2	E2
Absolute mean	me	Energy ratio3	E3
Pulse factor	va	Energy ratio4	E4
Kurtosis value	Kr	Energy ratio5	E5
Margin factor	L	Energy ratio6	E6
Peak factor	C	Energy ratio7	E7
Waveform factor	S	Energy ratio8	E8

peak-to-peak eigenvalues will be formed: PK = $\{x_1, x_2, ...x_{16}\}$.

The comparison sample set of other characteristic parameters is also established. The analysis results of 8 sets of health data and 8 sets of fault data of sensor 1 are shown in Table 3.

5. Reference Epidemic Cluster Analysis

Manifold learning is a unique machine learning method. Popular feature learning methods are divided into linear learning and nonlinear learning [22]. Its essence is that the sample points in the high-dimensional space are expanded into a manifold by a few main independent variables acting on the measurement space at the same time, and manifold learning is to pick up the low-dimensional manifolds embedded in the high-dimensional observation space. The essential characteristics of the data are found from the observation space to establish a new mapping relationship. Different from other feature extraction methods, manifold learning will maximize the local structure of high-dimensional raw data when obtaining the most similar low-dimensional embedded feature data of the original data. It realizes the learning and enhancement of data features and essential information, which also leads to the great advantage of manifold learning in mining and enhancing the essential information of data [23].

The comparison sample feature set N analyzed in this paper (N represents 16 feature sets composed of 16 feature parameters, such as PK, etc.) is an analysis model that integrates health samples with fault samples. Therefore, in this paper, when comparing the cluster analysis of the sample set, we need to combine the health samples for possession analysis. Therefore, to better find out the clustering distribution law of the reference sample feature set based on maintaining the local relation mechanism of the original parameter sample feature set, this paper uses a locally linear embedding LLE manifold learning method to construct the mapping relationship between the reference sample feature set and the clustering results. Thus, through the analysis of clustering results, the distinguishing relationship between health number and fault data in different eigenvalues is obtained.

LLE manifold learning uses the different weight information of the local neighborhood and adjacent points of each point, describes the local geometric features of the data through the local linear projection information, and finally realizes the expression and reconstruction of the local information of the sample globally [24–27].

LLE manifold learning computing process: On the same device, the data collected in the same location or in the same period have certain weight information between each other. LLE manifold learning methods use this weight information to construct the weight information subspace of the data group by establishing the neighborhood of each group of data. Then, through the dimensionality reduction analysis of the data set, the information of the multidimensional data set can be expressed and reconstructed in the low-dimensional space.

For high-dimensional feature sets $N = \{n_1, n_2, n_3, ..., n_i\} n_i \in R^{D\times m}$, the sensitive features of feature set N will be expressed in a low-dimensional d-dimensional space. The purpose of LLE algorithm is to obtain this low-dimensional embedded subspace $Y = \{y_1, y_2, y_3, ..., y_i\} y_i \in R^{d\times m}$. The manifold learning steps for LLE are divided into three steps as shown in the following figure.

(1) Construct the nearest neighbor space

The k nearest neighbors of each sample point are found according to the high-dimensional features and the Euclidean distance between each sample point n_i in N:

$$N_i = \mathrm{knn}(n_i, k), N_i = [n_{1i}, \cdots n_{ik}]. \tag{1}$$

(2) Calculate local weight

By calculating the nonlinear relationship between each sample and its nearest neighbor subspace, the local error function $\varepsilon(W)$ is minimized. The construction of the local weight matrix W is completed.

$$\begin{aligned}\varepsilon(W) &= \sum_{i=1}^{m}\left\|n_i - \sum_{j=1}^{k} w_{ij} n_j\right\|^2 \\ &= \sum_{i=1}^{m}\left\|\sum_{j=1}^{k}(n_i - n_{ji}) w_{ji}\right\|^2 \\ &= \sum_{i=1}^{m}\left\|(N - N_i) w_i\right\|^2 \\ &= \sum_{i=1}^{m} w_i^T (N - N_i)^T (N - N_i) w_i.\end{aligned} \tag{2}$$

Table 3: Time-frequency analysis results of vibration data of sensor 1.

Parameters	Health data							Fault data							
pk	7.06	7.130	7.22	6.18	13.95	6.459	8.835	7.228	32.27	29.51	27.59	30.77	24.20	36.61	27.04	32.67
st	1.38	1.441	1.32	1.24	2.004	1.265	1.509	1.323	4.50	4.77	3.75	4.57	4.27	3.57	3.47	3.91
me	1.14	1.191	1.10	1.05	1.558	1.063	1.227	1.103	3.20	3.40	2.71	3.22	3.09	2.51	2.50	2.80
va	6.14	5.987	6.55	5.88	8.957	6.077	7.199	6.555	10.08	8.68	10.17	9.54	7.82	14.58	10.83	11.67
Kr	6.05	6.788	5.46	4.31	19.20	4.627	8.359	5.465	101.3	109.3	71.20	110.2	82.06	81.30	66.60	82.48
L	6.93	6.767	7.39	6.61	10.37	6.846	8.193	7.392	12.55	10.85	12.44	11.97	9.65	17.96	13.21	14.37
C	5.11	4.949	5.46	4.96	6.963	5.104	5.854	5.462	7.18	8.18	7.36	6.73	5.67	10.26	7.80	8.35
S	1.20	1.21	1.20	1.185	1.286	1.190	1.230	1.200	1.40	1.40	1.38	1.42	1.38	1.42	1.39	1.40
E1	8.38	7.66	8.82	10.3	9.882	11.26	6.709	8.820	10.00	10.24	10.79	5.89	10.17	10.11	11.88	6.66
E2	6.51	6.57	6.29	5.83	8.954	5.044	7.308	6.293	12.54	12.63	11.96	14.04	14.89	15.90	10.26	14.97
E3	2.12	1.77	1.83	2.52	3.002	3.254	1.658	1.837	6.21	7.36	6.15	6.32	8.09	5.21	5.04	4.87
E4	8.24	8.92	7.74	7.55	9.833	6.451	9.834	7.740	12.07	11.98	10.05	11.97	11.50	10.90	9.63	11.56
E5	12.6	13.26	12.2	9.25	11.40	9.183	14.43	12.21	17.79	16.71	15.94	17.55	14.24	14.55	12.16	19.54
E6	37.37	33.72	39.91	46.21	31.30	46.52	29.06	39.91	12.45	11.89	20.41	9.39	18.08	18.11	19.12	10.54
E7	23.01	26.62	21.56	15.87	22.89	15.97	29.73	21.56	22.83	23.24	20.80	29.91	15.95	24.29	27.09	28.08
E8	1.732	1.439	1.614	2.359	2.725	2.303	1.264	1.614	6.11	5.94	3.90	4.93	7.07	0.92	4.82	3.78

Among them, N is a high-dimensional feature set. N_i is the k nearest neighbors of n_i, N_i is the nearest neighbor space in formula (1). w_{ij} is the weight between the sample n_i and the sample n_j. If this two are not nearest neighbors, then $w_{\mathrm{ij}} = 0$. Also, the weights of the nearest neighbor subspace of n_i satisfy the following equation:

$$\sum_{i=1}^{\mathrm{n}} w_{ij} = \sum_{j=1}^{k} w_i = 1. \tag{3}$$

According to the expression of formula (2), settings are as follows:

$$S_{\mathbf{i}} = (N - N_i)^T (N - N_i). \tag{4}$$

So,

$$\varepsilon(W) = w_i^T S_i w_i. \tag{5}$$

In order to obtain the optimal weight matrix, combined with the population dimensionality reduction analysis method, the Lagrangian multiplier method is adopted in this paper.

$$L(w_i) = \sum_{i=1}^{n} w_i^T S_i w_i + \lambda\left(w_i^T 1_k - 1\right). \tag{6}$$

The derivation of equation (6) is as follows:

$$\frac{\partial L(w_i)}{\partial w_i} = 2S_i w_i + \lambda 1_k = 0. \tag{7}$$

So,

$$w_i = \frac{S_i^{-1} 1_k}{1_k^T S_i^{-1} 1_k}. \tag{8}$$

Here, 1_k is a column vector of $k \times 1$ with all 1.

(3) Embedded coordinate projection

The embedded coordinate projection is to solve the mapping of the low space. First, we define a sparse matrix W of $n \times n$ cycles to represent w.

Therefore,

$$W = \{w_i = [w_{i1}, w_{i2}, \cdots w_{in}]\}^T. \tag{9}$$

So,

$$\sum_{j=1}^{n} w_{\mathrm{ji}} y_{\mathrm{ji}} = \sum_{j=1}^{k} w_{\mathrm{ji}} y_{\mathrm{ji}} = \mathrm{YW}_i. \tag{10}$$

After the abovementioned calculation, it is concluded that

$$\psi(Y) = \sum_{i=0}^{n} \left\| \left(Y\left(I_i - W_i\right)\right\right\|^2. \tag{11}$$

According to the matrix calculation formula,

$$\sum_{i} (a_i)^2 = \sum_{i} a_i{}^T a_i = \mathrm{tr}\left(\mathrm{AA}^T\right). \tag{12}$$

According to the formula (12), the simplified formula (11) is obtained.

$$\begin{aligned} \psi(Y) &= \mathrm{tr}\left(Y(I - W)(I - W)^T Y^T\right) \\ &= \mathrm{tr}\left(\mathrm{YMY}^T\right). \end{aligned} \tag{13}$$

Among them, $M = (I - W)(I - W)^T$.

By using Lagrange multiplier method, formula (13) is simplified as follows:

$$L(Y) = \mathrm{tr}\left(\mathrm{YMY}^T\right) + \lambda\left(\mathrm{YMY}^T - \mathrm{nI}\right). \tag{14}$$

The following equation is derived:

$$\frac{\partial L}{\partial Y} = 2\mathrm{YM} + 2\lambda \mathrm{Y} = 0. \tag{15}$$

Therefore,

$$M^T Y^T = -\lambda Y^T. \tag{16}$$

Because: $M^T = M$.
So,

$$MY^T = -\lambda Y^T. \tag{17}$$

Therefore, Y^T is a matrix composed of eigenvectors of matrix M. In order to reduce the dimension of data to d-dimension, we only need to obtain the smallest eigenvectors corresponding to d nonzero eigenvalues of M. In the process of LLE analysis, the smallest eigenvalue is generally discarded because it is too close to 0. Therefore, the eigenvector of the eigenvalue $[2, ..d + 1]$ from small to large is selected.

Sixteen multidimensional matrices composed of 16 eigenvectors are analyzed by LLE and selected $d = 2; k = 6$. The final analysis result is shown in Figure 6.

Through the analysis results obtained by LLE, we can see that peak-to-peak, kurtosis, waveform factor, and wavelet energy E2, E3, E6, and E8 can effectively separate the health signal from the fault signal. Effective value, mean square value, peak factor, and wavelet energy E1 can achieve data separation to a certain extent.

6. Linear Discriminant Analysis (LDA)

Linear discriminant analysis (LDA) is also known as Fisher discriminant analysis and class-based KLT [8]. This method selects the features that can best separate all kinds of data in the sense of least mean square so that the samples are as far away from each other in the feature space as possible and within the class as compact as possible, so that the sample has the best separability [28–30].

The principle of LDA is to protect the data to the low-dimensional space by projection, and the projected points will form a cluster by category, and the points of the same category will be projected to a closer space [31, 32]. A better distinction is made between different categories of data. By using this method, the interclass scatter matrix of the projected sample is maximum, and at the same time, the three-step matrix within the class is the smallest, so that different categories of data have the best separability in space.

The calculation process of LAD is as follows: Assuming that the projected vector is w, then for any sample x_i, its projection position is $w^T x_i$ on the projection, and u_1 and u_2 for different kinds of central points. The projection position on the projection is $w^T u_1$ and $w^T u_2$. The core of the LDA algorithm is to maximize $\|w^T u_1 - w^T u_2\|$, and the projection of the same class of data needs to be tighter and denser; that is, the data of the covariance of $w^T \sum_1 w + w^T \sum_2 w$ projection of the same class projection is as small as possible, so it is necessary to maximize the following formula:

$$\begin{aligned} J &= \frac{\left\|w^T u_1 - w^T u_2\right\|^2}{w^T \sum_1 w + w^T \sum_2 w} \\ &= \frac{w^T (u_1 - u_2)(u_1 - u_2)^T w}{w^T (\sum_1 + \sum_2) w}. \end{aligned} \tag{18}$$

So, the intraclass divergence is

$$\begin{aligned} S_w &= \sum_1 + \sum_2 \\ \sum_1 &= \sum_{i=1}^{X_1} (x_{1i} - u_1)(x_{1i} - u_1)^T \\ \sum_2 &= \sum_{i=1}^{X_2} (x_{2i} - u_2)(x_{2i} - u_2)^T. \end{aligned} \tag{19}$$

The divergence between classes is

$$S_B = (u_1 - u_2)(u_1 - u_2)^T. \tag{20}$$

So,

$$J = \frac{w^T S_B w}{w^T S_W w}. \tag{21}$$

General order in calculation is as follows:

$$w^T S_W w = 1. \tag{22}$$

Therefore, you need to maximize the value of $w^T S_B w$. Through the Lagrange multiplier method, it can be concluded that

$$S_B w = \lambda S_W w. \tag{23}$$

At the same time, because the direction of $S_B w$ is the same as the direction of $u_1 - u_2$; therefore,

$$w = {S_W}^{-1} (u_1 - u_2). \tag{24}$$

In this way, we get the best projection direction w of the original data.

After the abovementioned analysis, the analysis results of Section 5 are calculated by LDA projection. The final result is shown in Figure 7.

After LDA analysis, the health signal and fault signal of each eigenvalue is better segmented. Similar to the results of LLE analysis, the performance of peak-to-peak, kurtosis, waveform factor, and wavelet energy E2, E3, E6, and E8 in data separation is more prominent. The specific reasons are as follows: due to the damage of the gear, the impact of the cutting head of the roadheader is more unsmooth, which leads to a great change in the peak and peak value of the fault signal; the response of the kurtosis to the vibration is particularly obvious, so the fault signal can be represented effectively in the analysis. The damage of the reduction gear

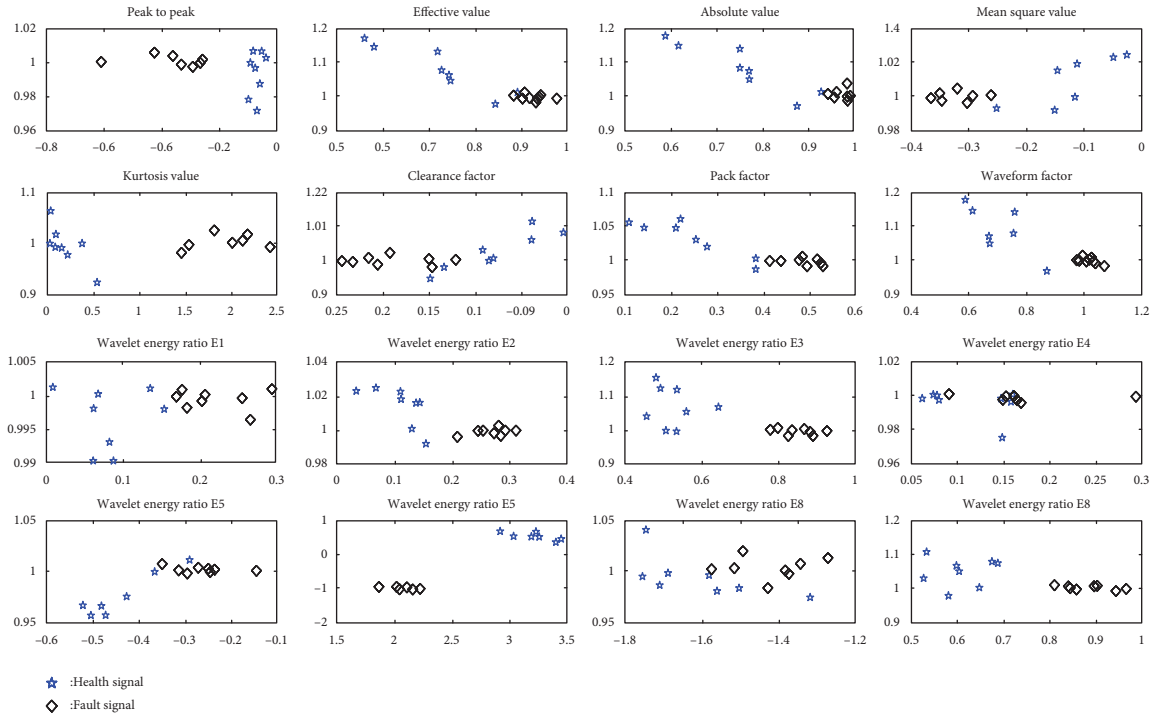

Figure 6: LLE analysis result.

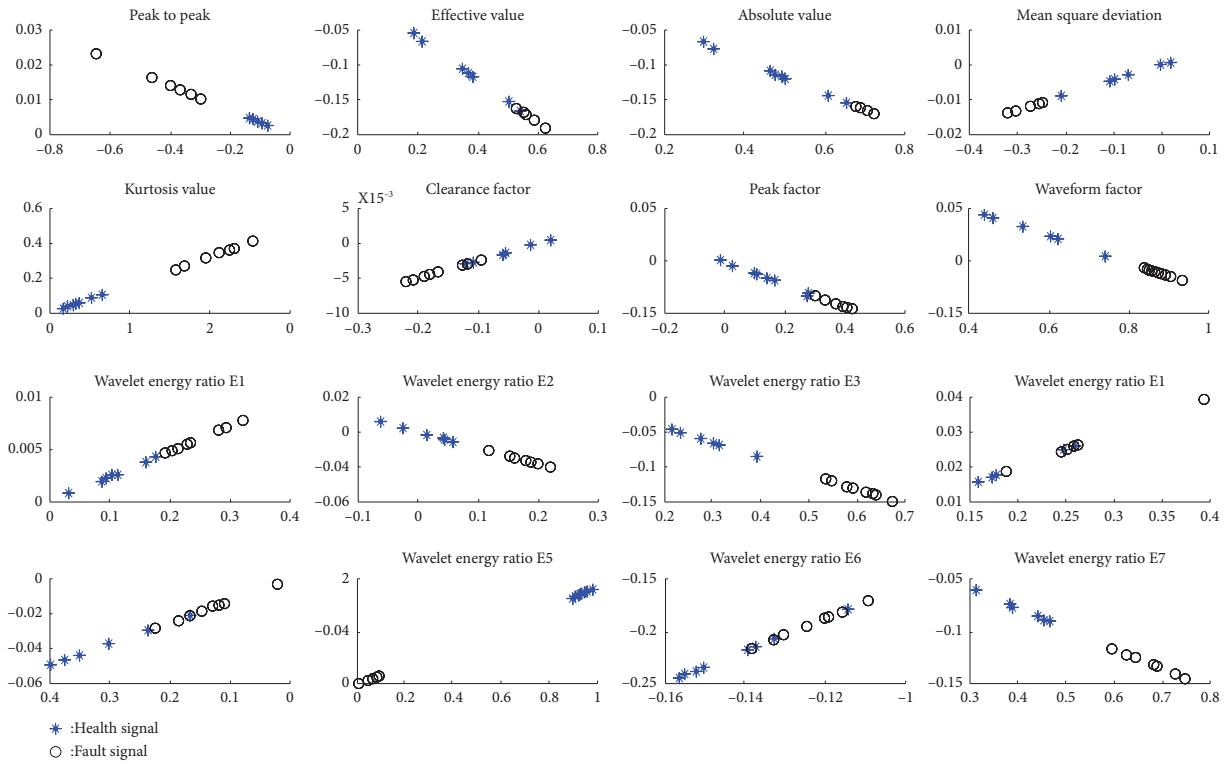

Figure 7: LDA analysis result.

in the cutting part of the roadheader leads to the vibration caused by the fault in addition to the working vibration in the working process of the roadheader, so its waveform factor will also change greatly. In the process of analyzing the wavelet energy parameters, the proportion of the low-frequency signal space E2 and E3 generated by the fault

increases, while the proportion of the high-frequency signal E6 of the gear operation becomes smaller obviously. At the same time, the frequency doubling signal generated by the fault also increases obviously in the high-frequency space.

7. Conclusion

In order to monitor the health status of roadheader, we proposed a vibration data analysis method based on LLE-LDA. First of all, the characteristic parameters are obtained by time-domain and wavelet analysis of the vibration sensor data of roadheader multimeasuring points. We composed the comparison samples set by using the characteristic parameters of different time points. Then, the dimension reduction of the sample set is compared by LLE. Finally, the LDA is carried out on the analyzed signal and the health signal. The difference between the analyzed signal and the health signal is compared through the analysis results. We can judge the health status of the roadheader. Through the vibration analysis, we can find that the health status and fault status can be effectively separated through the multimeasuring point and multiparameter analysis, even though complex environments can cause dramatic changes in load vibration. It not only provides technical support for the fault diagnosis of roadheader but also provides a reference for the analysis of fault types of large equipment. Compared with other fault analysis methods, this fault diagnosis method is more suitable for large equipment in complex working environment.

Data Availability

The data used to support the findings of this study are available from the corresponding author upon request.

Conflicts of Interest

The authors declare that they have no conflicts of interest.

Acknowledgments

The work was carried out by College of Intelligent Mines of the China University of Mining and Technology Beijing, Shijiazhuang Tiedao University and Jizhong Energy Group. This work was financially supported by the National Natural Science Foundation of China (Grant no. 51874308).

References

[1] S. Deshmukh, A. K. Raina, V. M. S. R. Murthy, R. Trivedi, and R. Vajre, "Roadheader– a comprehensive review," *Tunnelling and Underground Space Technology*, vol. 95, pp. 103148–103151, 2020.

[2] Y. U. Yue-sen, L. Y. U. Wei, and X. J. Wu, "Design on remote monitoring and fault diagnosis system of boomtype roadheader," *Coal Mine Machinery*, vol. 34, no. 8, pp. 299–301, 2013.

[3] M. Wu, L. I. Rui, and P. Wang, "Preliminary study on the parallel technology of fully mechanized roadway based on digital twin," *Journal of China Coal Society*, vol. 45, no. S1, pp. 506–513, 2020.

[4] J. Wang, G. Du, Z. Zhu, S. Changqing, and H. Qingbo, "Fault diagnosis of rotating machines based on the EMD manifold," *Mechanical Systems and Signal Processing*, vol. 135, no. 1, Article ID 106443, 2020.

[5] R. Comakli, "Performance of roadheaders in low strength pyroclastic rocks, a case study of cold storage caverns in Cappadocia," *Tunnelling and Underground Space Technology*, vol. 89, pp. 179–188, 2019.

[6] O. Acaroglu and C. Erdogan, "Stability analysis of roadheaders with mini-disc," *Tunnelling and Underground Space Technology*, vol. 68, pp. 187–195, 2017.

[7] J. Sun, J. Wang, F. Liang, and D. Kong, "Finite element analysis of the reducer case of the cutting part of the roadheader," *Coal Mining Machinery*, vol. 32, no. 8, pp. 79–81, 2011.

[8] B. Wang, "Experimental modal analysis of coal roadheader exciting vibration," *Coal Mine Electromechanical*, vol. 02, no. 009, pp. 19–21, 2008.

[9] Y. Hu, Y. Yang, and M. Wu, "Research on vibration intensity distribution of cantilever hard rock roadheader," *Industry and Mine Automation*, vol. 41, no. 8, pp. 35–37, 2015.

[10] J. J. Yang, Z. Tang, X. Wang, Z. Wang, and M. Wu, "Roadheader anomaly detection method based on VSAP-SO-BP under the single category learning," *Joural of vibration Measurement & Diagnosis*, vol. 39, no. 1, pp. 130–135, 2019.

[11] Y. Qu, X. Ji, and F. Lv, *Operating Modal Analysis of the Turntable on a Working Road-Header Using DTCWT*, Springer, Cham, Salmon Tower Building NY, USA, 2019.

[12] X. Ding, Q. Li, L. Lin, Q. He, and Y. Shao, "Fast time-frequency manifold learning and its reconstruction for transient feature extraction in rotating machinery fault diagnosis," *Measurement*, vol. 141, pp. 380–395, 2019.

[13] Z. Li, J. Chen, Y. Zi, and S. He, "A sensor-dependent vibration data driven fault identification method via autonomous variational mode decomposition for transmission system of shipborne antenna," *Sensors and Actuators A: Physical*, vol. 279, pp. 376–389, 2018.

[14] D. G. ChiragMongia and S. Shankar, "Vibration response-based condition monitoring and fault diagnosis of rotary machinery," *Neurocomputing*, vol. 434, pp. 98–125, 2021.

[15] X. Ding, *Research on Theory and Methodology of Manifold Feature Enhancement for Machine Condition Monitoring and Diagnosis*, University of Science and Technology of China, Hefei, Anhui, China, 2017.

[16] M. Zhang, X. Ji, L. I. Xu, Y. Qu, and M. Wu, "Model identification and precise control of the tunnel boring machine body posture adjustment," *Journal Of Xi'an Jiaotong University*, vol. 55, no. 6, pp. y1–y11, 2020.

[17] Y. Hu, *Study on Roadheader's Vibration Characteristics Based on Working Conditions in Coal Mine*, China University of Mining & Technology, Beijing, China, 2015.

[18] P. Zhang and X. Zhang, "Fault diagnosis of rotating machinery based on evidence theory of evidence entropy," *Joural of Vibration Measurement & Diagnosis*, vol. 30, no. 1, pp. 55–58, 2010.

[19] H. An and Z. H. A. O. Rongzhen, "CKLPMDP algorithm for dimension reduction of a rotor fault data set," *Journal of Vibration and Shock*, vol. 40, no. 9, pp. 37–54, 2021.

[20] W. Zhang, C. Li, T. Huo, X. Qu, and C. Xin, "Vibration events in underground heading face and useful index for rock burst monitoring," *Measurement*, vol. 180, Article ID 109501, 2021.

[21] A. Ch, B. Ama, and B. Mdmoa, "Necessity of imposing total miscibility for certain binary pairs in lle data correlations," *Fluid Phase Equilibria*, vol. 538, 2021.

[22] A. Sr and B. Nk, "Coupling VOF interfacial mass transfer model with RSM approach in LLE systems: developing the new correlations for mass transfer, aspect ratio and terminal velocity- ScienceDirect," *International Communications in Heat and Mass Transfer*, vol. 123, 2021.

[23] Y. Yu, S. Wang, and L. Zhang, "Stock price forecasting based on bp neural network model of network public opinion," in *Proceedings of the 2017 2nd International Conference on Image, Vision and Computing (ICIVC)*, June 2017.

[24] F. Anowar and S. Sadaoui, "Conceptual and empirical comparison of dimensionality reduction algorithms (PCA, KPCA, LDA, MDS, SVD, LLE, ISOMAP, LE, ICA, t-SNE)," *Computer Science Review*, vol. 40, 2021.

[25] X. Cui, Q. Wang, W. E. I. Kai, T. E. N. G. Geer, and X. U. Xiangjun, "Laser-induced breakdown spectroscopy for the classifification of wood materials using machine learning methods combined with feature selection," *Plasma Science and Technology*, vol. 23, no. 05, pp. 1–9, 2021.

[26] D. Lei, Q. Li, Y. Chen, X. Ding, and W. Huang, "Shao Yimin Complex scale feature extraction for gearbox via adaptive multi-mode manifold learning," *MeasurementVolume*, vol. 174, 2021.

[27] Z. Li, Y. Cao, H. Peng, and F. Meng, "Smart grid fault location based on manifold theory and L1+L2 constraints," *Power System Protection and Control*, vol. 48, no. 18, pp. 48–57, 2020.

[28] W. Li, L. Sun, and D. Zhang, "Text classification based on labeled-LDA model," *Chinese Journal of Computers*, vol. 31, no. 4, pp. 620–624, 2018.

[29] J. Xu, Z. Wu, Y. Xu, and J. Zeng, "Face recognition based on PCA、LDA and SVM algorithms," *Computer Engineering and Applications*, vol. 46, no. 32, pp. 17–21, 2010.

[30] R. Joshi, R. Prasad, P. Mewada, and P. Saurabh, "Modified LDA approach for cluster based gene classification using K-mean method," *Procedia Computer Science*, vol. 171, pp. 2493–2500, 2020.

[31] K. S. Gyamfi, J. Brusey, A. Hunt, and E. Gaura, "A dynamic linear model for heteroscedastic LDA under class imbalance," *Neurocomputing*, vol. 343, pp. 65–75, 2019.

[32] L. I. U. Zhong-bao and S. T. Wang, "Improved LDA algorithm and research on rank limitation," *Computer Engineering and Applications*, vol. 46, no. 32, pp. 17–20, 2010.